Life Sciences 226 (2019) 22–32

Contents lists available at ScienceDirect

Life Sciences

journal homepage: www.elsevier.com/locate/lifescie

GPR 30 reduces myocardial infarct area and fibrosis in female ovariectomized mice by activating the PI3K/AKT pathway

Xiaowu Wang[a,1], Linhe Lu[a,1], Yanzhen Tan[a], Liqing Jiang[a], Minggao Zhao[b], Erhe Gao[c], Shiqiang Yu[a], Jincheng Liu[a,*]

[a] Cardiovascular Surgery, Xijing Hospital, Fourth Military Medical University, Xi'an 710032, PR China
[b] Department of Pharmacology, School of Pharmacy, Fourth Military Medical University, Xi'an 710032, PR China
[c] Center for Translational Medicine, Lewis Katz School of Medicine at Temple University, Philadelphia, PA 19140, USA

ARTICLE INFO

Keywords:
G-protein coupled estrogen receptor 30 (GPR30)
Myocardial infarction (MI)
Ovariectomy
Cardiac fibroblasts
Hypoxia/serum deprivation (H/SD)
Cardioprotection

ABSTRACT

Aims: Estrogen plays an important role in cardioprotection. Animal experiments showed that the G-protein coupled estrogen receptor 30 (GPR30) specific agonist G1 could reduce post-ischemic dysfunction and inhibit cardiac fibroblast proliferation. However, the underlying mechanism of action is not clear. The current study tests the hypothesis that GPR30 reduces myocardial infarct area and fibrosis in female ovariectomized (OVX) mice by activating the PI3K/AKT pathway.

Main methods: In this study, we established a myocardial infarction (MI) animal model derived from OVX C57BL/6 female mice, and investigated the effect of G1 on cardiac function by echocardiography and Hemodynamics, morphology and expression of fibrosis-related and apoptosis-related proteins by Masson's trichrome and H&E, Immunofluorescence, Western blotting and TUNEL.

Key findings: Combination with OVX significantly increased myocardial fibrosis and MI area compared to MI treatment alone, as determined by echocardiography and hemodynamics. Further addition of G1 changed the expression of apoptosis-related proteins, decreased the levels of tumor necrosis factor-α and interleukin-10, and reduced the degree of myocardial fibrosis and myocardial infarct area. Primary cultured cardiac fibroblasts (CFs) were subjected to hypoxia/serum deprivation (H/SD) simulating the in vivo ischemia model. When the PI3K/AKT pathway was inhibited by wortmanin in H/SD CFs, G1 failed to induce significant changes in the expression of apoptosis-related proteins.

Significance: It suggested that GPR30 may improve cardiac function in female OVX mice by activating the PI3K/AKT pathway and reducing myocardial infarct size and fibrosis.

1. Introduction

Myocardial infarction (MI) is a common cardiovascular disease. Epidemiological surveys have shown that women younger than 55 years of age rarely have MI, and the incidence in perimenopausal and postmenopausal women shows an apparent difference [1]. Compared with elderly men, elderly women have more severe fibrosis in ischemic heart disease [2]. The considerable decrease in estrogen in postmenopausal women leads to reduced cardioprotection and increased risk for cardiovascular disease [3], but estrogen treatment has no apparent effect in such cases [4]. Studies on animal models have shown that the G-protein coupled estrogen receptor 30 (GPR30) specific agonist G1 reduced post-ischemic dysfunction and inhibited cardiac fibroblast proliferation [5].

GPR30, also known as GPER, is a new estrogen receptor (ER) that binds estrogen with high affinity and regulates cell proliferation [6]. Chronic activation of GPR30 with agonist G1 attenuates heart failure, and confers cardioprotection and improvement of cardiac function [7,8]. Bopassa et al. [5] demonstrated that pretreatment with the GPR30 agonist G1 during isolated heart perfusion in MI mice significantly reduced the infarct size. However, the precise mechanism underlying the action of GPR30 remains unclear.

The inflammatory reaction and apoptosis induced by MI play an important role in the development and prognosis of the disease and are crucial factors for ventricular remodeling after MI. Inhibition of inflammation and apoptosis has become an important link in the

* Corresponding author.
E-mail address: labaniz@fmmu.edu.cn (J. Liu).
[1] These authors contributed to this work equally.

https://doi.org/10.1016/j.lfs.2019.03.049
Received 24 December 2018; Received in revised form 14 March 2019; Accepted 20 March 2019
Available online 21 March 2019

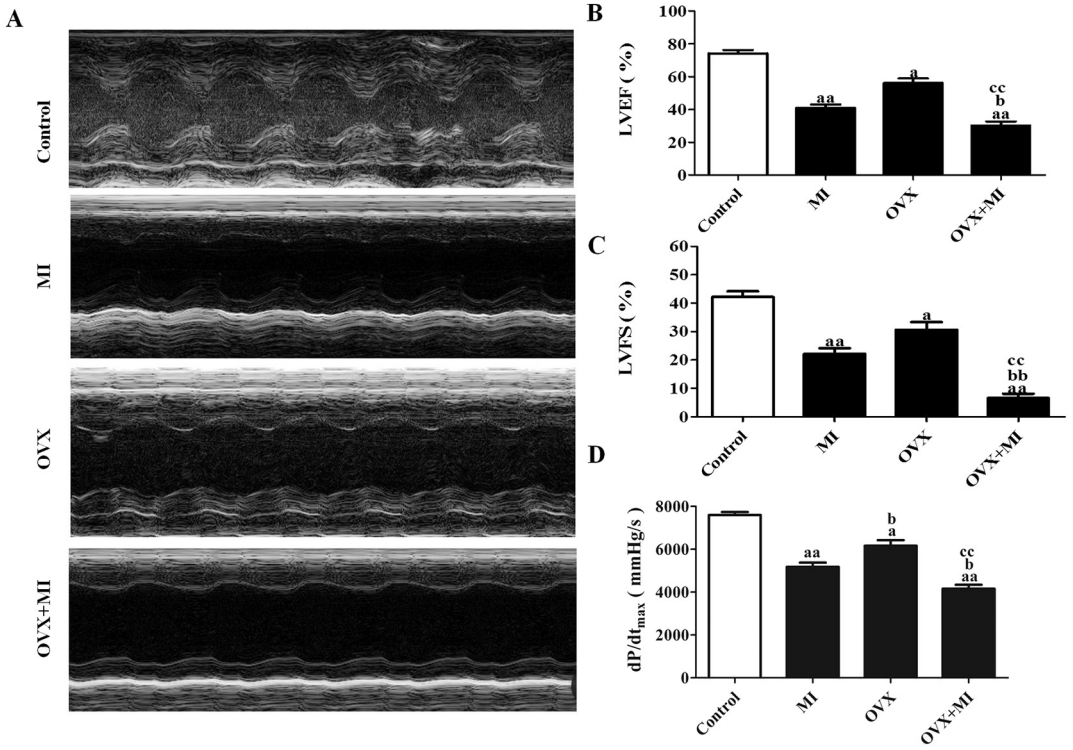

Fig. 1. Effect of ovariectomy on cardiac function of female mice with MI. Mice underwent myocardial infarction (MI) surgery 2 weeks after they were ovariectomized (OVX), and M-mode ultrasonography and hemodynamic tests were performed 4 weeks thereafter. (A) Representative M-mode images by echocardiography for MI, OVX and OVX + MI group (B) Left ventricular ejection fraction (LVEF) of A (C) Left ventricular fractional shortening (LVFS) of A (D) Hemodynamic analysis for MI, OVX and OVX + MI group. The results are expressed as mean ± S.E.M., n = 6, $^{a}p < 0.05$ and $^{aa}p < 0.01$ compared with control group. $^{b}p < 0.05$ and $^{bb}p < 0.01$ compared with MI group. $^{c}p < 0.05$ and $^{cc}p < 0.01$ compared with OVX group.

prevention of ventricular remodeling and adjustment of cardiac dysfunction in MI [9]. The PI3K/AKT pathway plays an important role in regulating inflammation and apoptosis [10]. Inflammation after ischemic reperfusion (IR) plays a key role in the extension of myocardial IR injury. Cardioprotection from IR injury could be induced via activation of PI3K pathway and inhibition of inflammation [11]. Cardiomyocyte apoptosis, which occurs during ischemia and reperfusion injury, can cause irreversible damage to cardiac function. Such as nuclear factor 45 (NF45) was shown to prevent hypoxia-reoxygenation (H/R)-induced H9c2 cell apoptosis via PI3K/Akt pathway [12]. However, it is unclear whether GPR30 activates the PI3K/AKT pathway to reduce the apoptosis and inflammatory response of myocardial tissues in ovariectomized (OVX) mice with MI.

Therefore, in this study, we selected OVX female C57BL/6 mice and primary cultured cardiac fibroblasts (CFs) to establish an animal model of MI and a hypoxia/serum deprivation (H/SD) cell model simulating the in vivo ischemia condition, respectively [13]. We treated these models with the GPR30 agonist G1 to observe the change in apoptosis-related protein expression, apoptosis rate, tumor necrosis factor-α (TNF-α) and interleukin-10 (IL-10) levels, cardiac function, myocardial infarct size, and myocardial fibrosis. Furthermore, we investigated the effect of GPR30 on PI3K/AKT signaling molecules to explore the related mechanisms of GPR30 in reducing myocardial infarct size and rescuing the necrotic myocardial tissues in OVX female mice with MI. We hypothesized that GPR30 may improve cardiac function in female OVX mice by activating the PI3K / AKT pathway and reducing myocardial infarct size and fibrosis.

2. Materials and methods

2.1. Materials

The GPR30 agonist, G1, and PI3K inhibitor, wortmanin, were purchased from Cayman Chemical (Ann Arbor, MI, USA). The TUNEL assay kit was obtained from Roche Diagnostics GmbH (Bayer, Mannheim, Germany). The BCA protein quantification kit was purchased from Merck Millipore Technology (Darmstadt, Germany). The primary antibodies against GPR30 (ab39742), TGF-β1 (ab92486), collagen I (ab34710), BAX (ab32503), BCL-2 (ab196495), caspase-3 (ab4051), p-AKT (ab81283), total AKT (ab32505), Vimentin (ab92547), Troponin (ab47003) and α-SMA (ab5694) were purchased from Abcam (USA). Antibodies against GAPDH and β-actin were obtained from Santa Cruz Biotechnology (Santa Cruz, CA, USA). Tumor necrosis factor-α (TNF-α) and interleukin-10 (IL-10) detection kits were purchased from Elabscience Bioengineering Institute WuHan (China), and DAPI was obtained from Roche Molecular Biochemicals (Bayer, Mannheim, Germany).

2.2. Animal model and treatment

Female eight-week-old C57BL/6 mice weighing 20–24 g were purchased from the Center of Experimental Animal in the Fourth Military Medical University (FMMU), China. Mice were randomly divided into the following five experimental groups, with n = 20 for each group: 1) control group, 2) MI group, 3) OVX group, 4) OVX + MI group, and 5) OVX + MI + G1 group. All animal experiments were approved by the AFMU Committee of Animal Care (No. 20170203).

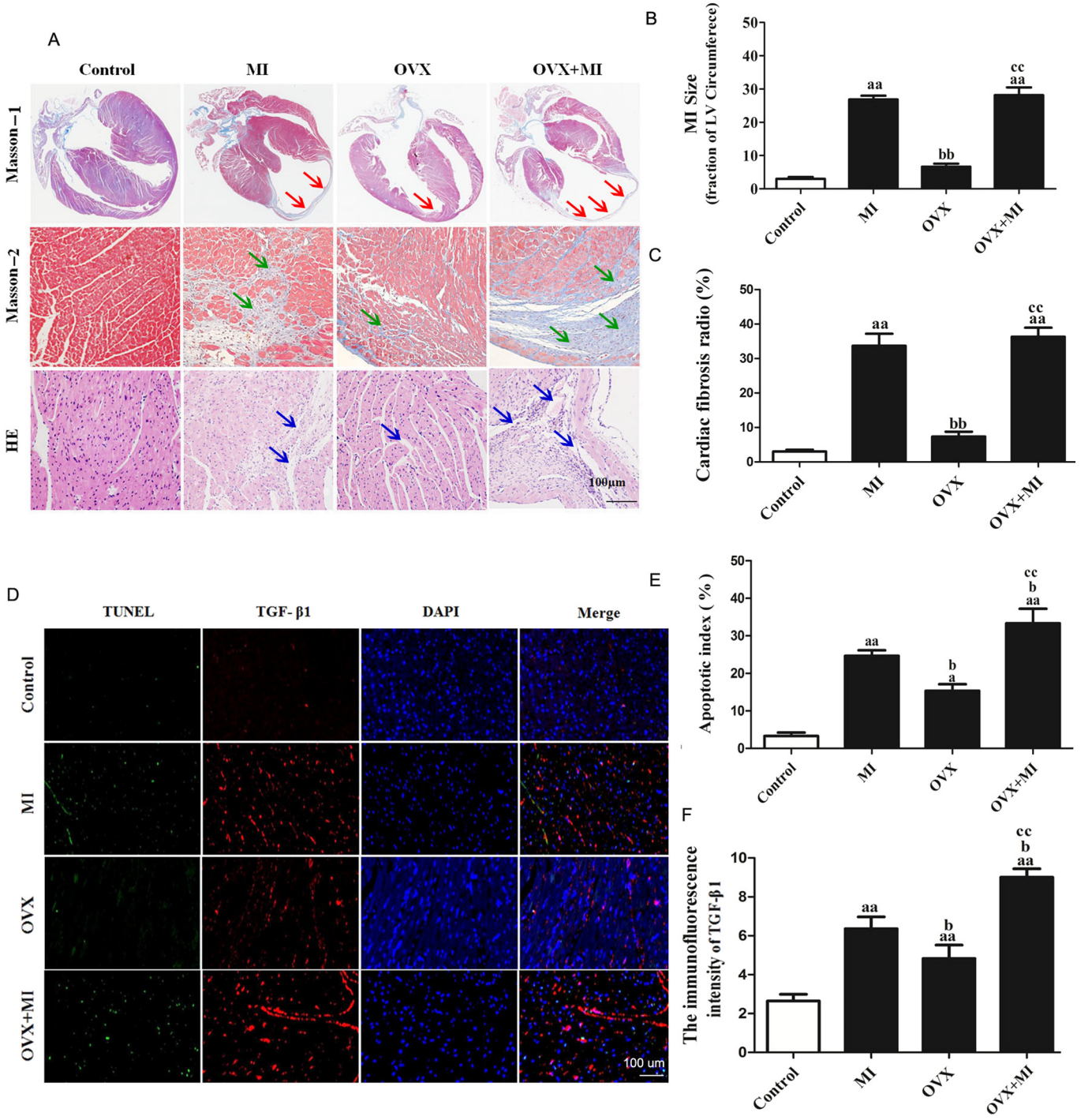

Fig. 2. Changes in cardiac fibrosis and morphology in OVX female mice with MI. (A) Cardiac Masson's trichrome and H&E staining. (Bar = 100 μm for Masson-2 and H&E, thinner ventricular wall were indicated by red arrows, fibrosis increase area were indicated by green arrows, tissue loose area were indicated by blue arrows.). (B) Infarct size (fraction of left ventricle (LV) circumference). (C) Cardiac fibrosis %. (D) Representative photomicrographs of in situ detection of apoptotic cardiomyocytes by TUNEL staining. Red fluorescence shows TGF-β1 expression. Green fluorescence shows TUNEL-positive nucleus. Blue fluorescence shows nuclei of total cardiomyocytes (Bar = 100 μm). (E) Percentage of TUNEL-positive nuclei. (F) IFC intensity. The results are expressed as the mean ± S.E.M., n = 8. $^{a}p < 0.05$ and $^{aa}p < 0.01$ compared with control group. $^{b}p < 0.05$ compared with MI group. $^{cc}p < 0.01$ compared with OVX group. (For interpretation of the references to color in this figure legend, the reader is referred to the web version of this article.)

2.3. Ovariectomy and MI induction

Bilateral ovariectomy was performed on C57BL/6 mice after being anesthetized in an induction chamber with 2% isoflurane mixed with pure oxygen (0.5–1.0 L/min). MI was induced in mice 2 weeks after the bilateral ovariectomy (OVX + MI mice). To establish MI injury, the left anterior descending coronary artery of mice was occluded using a 6-mm silk suture [14]. Control animals underwent the same [15] surgery without ligation of the coronary artery. After MI surgery, G1 (35 μg/kg/d) was intraperitoneally injected for 4 weeks [16–18], whereas mice in groups 1–4 were injected with an equal volume of vehicle solution (DMSO:PBS(V/V) = 1:99) at the same intervals.

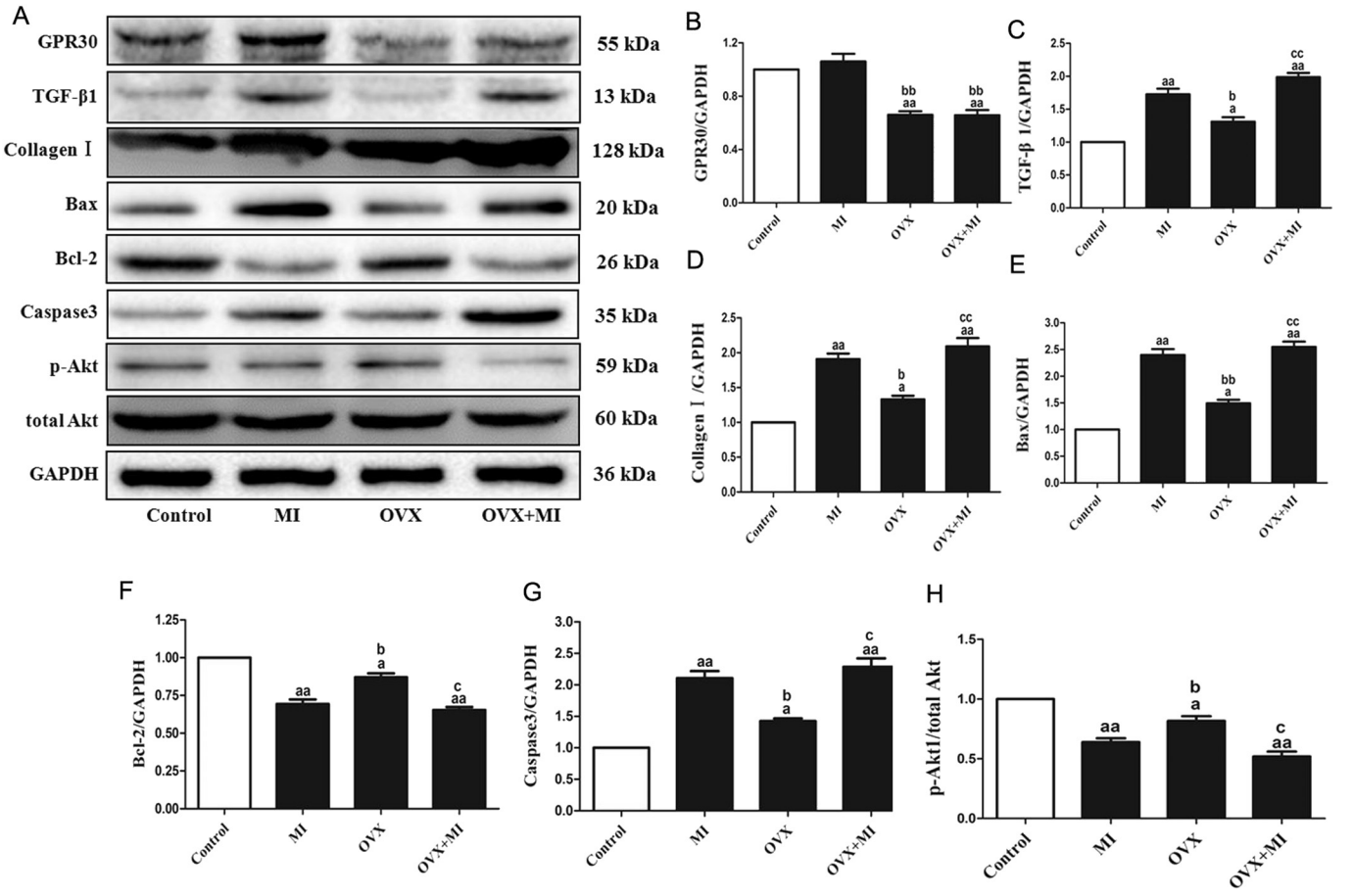

Fig. 3. Western blot analysis for expression of G-protein coupled estrogen receptor 30 (GPR30), TGF-β1, collagen I, BAX, BCL-, caspase-3, p-AKT, and total AKT in different treatment groups. (A) Representative blots. (B) GPR30 expression. (C) TGF-β1 expression. (D) Collagen I expression. (E) BAX expression. (F) BCL-2 expression. (G) Caspase 3 expression. (H) p-AKT/AKT ratio. The results are expressed as mean ± S.E.M., n = 8/group. $^{a}p < 0.05$ and $^{aa}p < 0.01$ compared with control group. $^{b}p < 0.05$ and $^{bb}p < 0.01$ compared with myocardial infarction (MI) group. $^{c}p < 0.05$ and $^{cc}p < 0.01$ compared with OVX group.

2.4. Echocardiographic measurement

Two-dimensional and M-mode echocardiographic measurements were performed with a VEVO 770 high-resolution in vivo imaging system (VisualSonics, Toronto, ON, Canada). The ultrasound data were measured 3 days before (baseline) and 4 weeks after MI operation as described previously [19]. Echocardiographic assessment was performed under anesthesia via isoflurane inhalation (1% to 2%) and at a controlled heart rate (≥500 bpm) and body temperature (37 ± 1)°C. Endocardial volumes during diastole and systole were recorded from bidimensional long-axis parasternal views.

2.5. Hemodynamics

Hemodynamic analysis was performed at 4 weeks post MI via miniaturized pressure-volume catheterization, as previously described [20]. A tipped catheter (SPR-839; Millar Instruments, Houston, USA) was inserted into the right carotid artery and advanced retrograde into the left ventricle (LV) in the anesthetized mice (1% to 2% isoflurane inhalation). LV pressure-volume loops were recorded at steady state and at varying preloads during temporary compression of the inferior vena cava. After inferior vena cava compression, isoproterenol (ISO; 40 ng/kg/min) was injected into the left jugular vein, and the analysis was repeated. All analyses were performed using LabChart 7 software [21].

2.6. Morphometric analyses

Following MI, heart left ventricular was removed and fixed with 4% paraformaldehyde, and transverse sections were cut. Cross sections (4 μm thick) were stained with Masson's trichrome and H&E. Infarct size was measured using Masson's trichrome-stained sections, as previously described [22]. Infarct size was calculated as the percentage of LV circumference occupied by the infarct scar. The degree of cardiac fibrosis was determined based on the area of fibrosis divided by the total area (% cardiac fibrosis) by using BIOQUANT image analysis software [23].

2.7. Immunocytochemistry and TUNEL assay

Immunohistochemistry staining of formalin-fixed and paraffin-embedded heart left ventricular sections was performed using standard procedures. The fixed fibroblasts were incubated overnight with primary anti-TGF-β1 (1:200) at 4 °C, and then incubated with Cy3-conjugated goat anti-rabbit IgG (1:100 dilution) in blocking solution. TUNEL detection solution was added to the sections, and the sections were incubated at 37 °C in the dark for 2 h. Nuclear staining was performed with DAPI. The stained samples were analyzed using an Olympus Fluoview FV1000 microscope (Olympus, Japan); cells from ten randomly selected visual fields in each section were counted to determine the apoptotic index. Myocardial apoptosis was analyzed by TUNEL assay using an in situ cell death detection kit, as previously described [24]. Images of Immunofluorescence (IF) were captured digitally in five random microscope fields from each sample and were

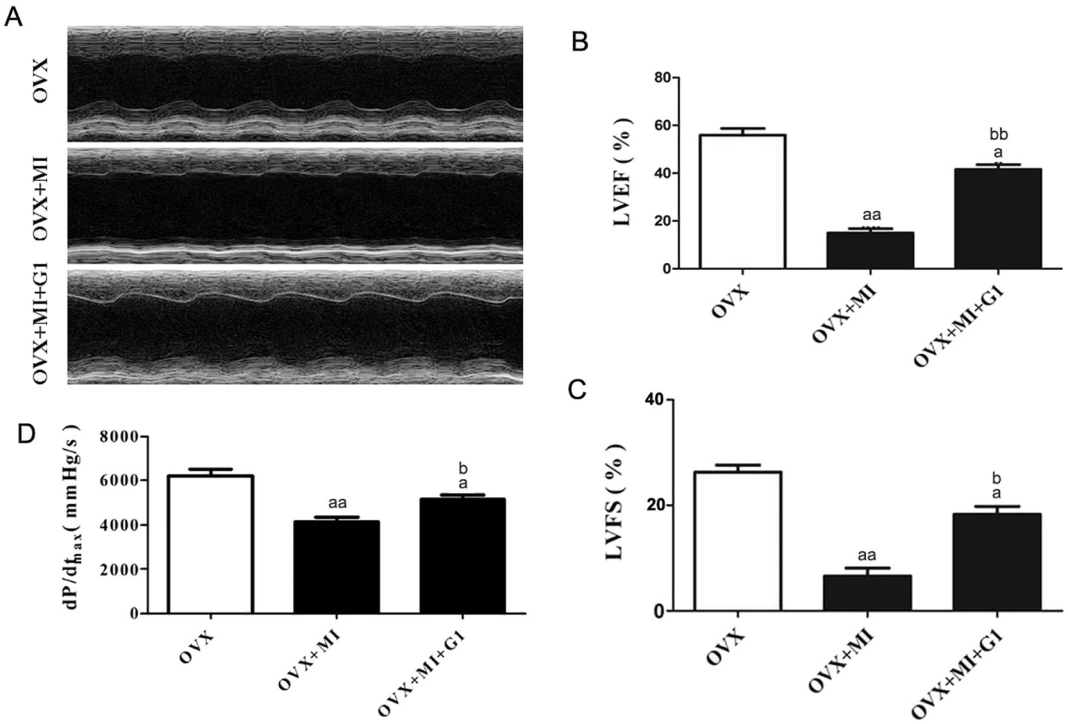

Fig. 4. Effect of GPR30 agonist G1 on cardiac function of female mice with MI. Mice underwent MI surgery 2 weeks after they were OVX, and then, G1 was intraperitoneally injected for 4 weeks. (A) M-mode ultrasonography tests were performed Representative M-mode images by echocardiography (B) LVEF of E (C) LVFS of E. (D) Hemodynamic analysis for OVX, OVX + MI and OVX + MI + G1 group. The results are expressed as mean ± S.E.M., n = 6, $^{a}p < 0.05$ and $^{aa}p < 0.01$ compared with OVX group. $^{b}p < 0.05$ and $^{bb}p < 0.01$ compared with OVX + MI group.

analyzed with analysis software (Image Pro-Plus; Image Solutions, Torrance, CA, USA). The index of apoptosis was expressed as the ratio of positively stained apoptotic myocytes to the total number of myocytes counted ×100% [25].

2.8. Western blotting (WB)

Heart was harvested and protein was extracted from left ventricular tissue for Western blotting. The primary antibodies used for WB were against GPR30, TGF-β1, collagen I, BAX, caspase 3, BCL-2, p-Akt, total Akt, and GAPDH. The positive protein bands were developed using a chemiluminescent system, and the bands were scanned and quantified by densitometric analysis performed using a Quantity One (Bio-Rad, Richmond, CA, USA) image analyzer.

2.9. Determination of the inflammatory relative cytokines TNF-α and IL-10

To observe the change in inflammatory relative cytokines in different groups, MI was induced in mice 2 weeks after the bilateral ovariectomy (OVX + MI mice). Then, G1 (35 μg/kg/d) was intraperitoneally injected for 2 weeks. We collected the serum of different groups to test the level of TNF-α and IL-10 using commercially available sandwich ELISA kits (R&D Systems, USA), as described previously [26].

2.10. CF culture and H/SD injury to simulate MI in vivo

CFs of mice were collected and ventricular myocytes were isolated, as previously described [27]. The purity of cultured CFs was determined as > 98% by immunohistochemistry based on the expression of the CF marker vimentin. Immunopositive cells from passages 3–5 were used for experiments. Before each experiment, the cells were seeded in 6-well plates or a laser confocal microscopy dish at a density of 3×10^4 cells/cm^2 in DMEM containing 10% fetal bovine serum and cultured for 24 h. The H/SD injury cell model was used to mimic MI in vivo, as previously described [28,29]. Briefly, after the indicated treatment, primary cultured CFs were exposed to hypoxia (94% N_2, 5% CO_2, and 1% O_2) in an anaerobic system (Thermo Forma, USA) at 37 °C for the indicated duration in Hank's buffer [29].

2.11. Cell viability assay

CFs were seeded in a 96-well culture plate. CFs were treated with H/SD, H/SD + G1 (10 nM) [30], H/SD + Wortmanin (100 nM) [31], and H/SD + G1 + Wortmanin, and cell viability was measured using the 3-(4,5-dimethylthiazol-2-yl) -2,5- diphenyltetrazolium bromide (MTT) assay [32]. Briefly, after treatment, CFs were washed with phosphate-buffered saline and incubated with 10 μl of MTT reagent (final concentration of 0.5 mg/ml) for 4 h. Then, 100 μl of DMSO was added to dissolve the formazan crystals, and the absorbance at 490 nm was measured using a SpectraMax 190 microtiter plate reader (Molecular Devices, Sunnyvale, CA, USA). Cell viability was calculated by dividing the optical density of samples by that of the control group.

2.12. Statistical analysis

All experiments were performed in triplicate. All values are presented as the mean ± S.E.M. Differences were compared by ANOVA followed by Bonferroni correction for post hoc *t*-test, where appropriate. All statistical tests were performed using the GraphPad Prism software, version 5.0 (GraphPad Software Inc., San Diego, CA, USA). Differences with $p < 0.05$ were considered statistically significant.

3. Results

3.1. Effect of ovariectomy on cardiac function of female mice with MI

M-mode ultrasonography results of different groups are shown in

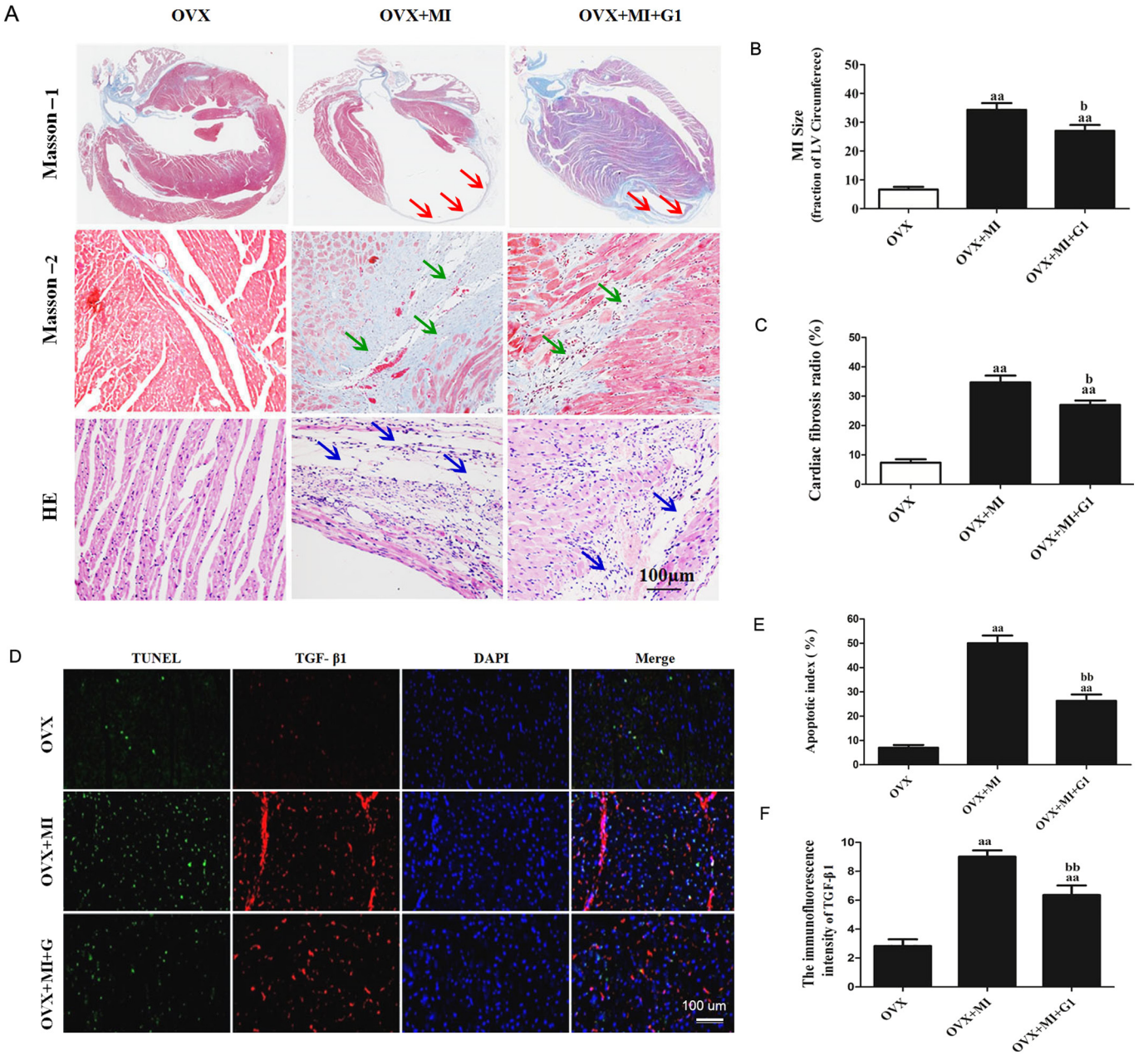

Fig. 5. Effect of GPR30 agonist G1 on the degree of fibrosis and cardiac morphology in OVX female mice with MI. (A) Masson's trichrome staining and H&E staining to observe the changes in cardiac fibrosis and histomorphology after MI surgery (bar = 100 μm for Masson-2 and H&E, thinner ventricular wall were indicated by red arrows, fibrosis increase area were indicated by green arrows, tissue loose area were indicated by blue arrows.). (B) Infarct size (fraction of LV circumference). (C) Cardiac fibrosis %. (D) Representative photomicrographs of in situ detection of apoptotic cardiomyocytes by TUNEL staining. Red fluorescence shows TGF-β1 expression. Green fluorescence shows TUNEL-positive nucleus. Blue fluorescence shows nuclei of total cardiomyocytes (bar = 100 μm). (E) Percentage of TUNEL-positive nuclei. (F) IFC intensity. The results are expressed as the mean ± S.E.M., n = 8/group. $^{a}p < 0.05$ and $^{aa}p < 0.01$ compared with the OVX (OVX) group. $^{b}p < 0.05$ and $^{bb}p < 0.01$ compared with the OVX + MI group. (For interpretation of the references to color in this figure legend, the reader is referred to the web version of this article.)

Fig. 1. The LVEF values in the OVX group were significantly lower than those in the control group ($p \leq 0.05$), whereas those in the OVX + MI group showed a further decrease ($p \leq 0.05$ vs. MI group; Fig. 1B). Similar trends were observed for LVFS values among the different groups (Fig. 1C). Lower dP/dt max values were detected in both the MI group and OVX group ($p \leq 0.01$ and $p \leq 0.05$ vs. control group, respectively) by hemodynamic analysis. Treatment with OVX or OVX + DM further decreased the dP/dt max values ($p < 0.01$; Fig. 1D). All of these results indicate that OVX and MI reduce cardiac function in mice, and that OVX combined with MI further aggravates cardiac function injury.

3.2. Effect of ovariectomy on cardiac morphology of female mice with MI

The whole heart tissue of mice of the different groups was fixed in 10% formalin and stained with Masson's trichrome to calculate the ratio of scar tissue size to left ventricular wall area (Fig. 2A). MI surgery caused the ventricular wall to become thinner; additionally, the degree of fibrosis increased, and edema appeared on the edge of the infarct area. Similarly, the OVX treatment group showed thinner heart tissue and ventricular wall and a higher degree of myocardial fibrosis. The ventricular wall became thinner in the infarct area with a high degree of fibrosis in the OVX + MI group compared to the MI group (Fig. 2B

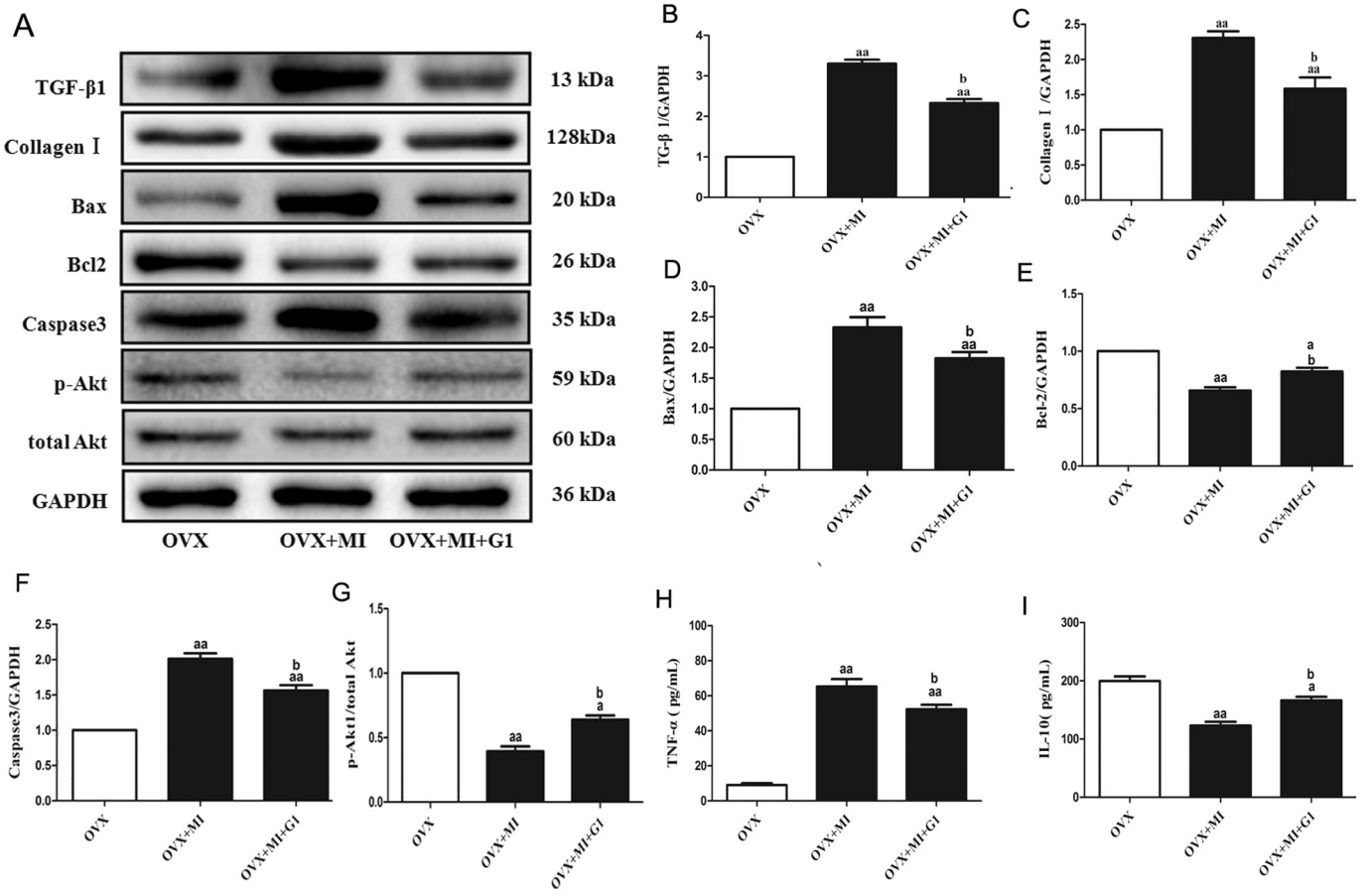

Fig. 6. Effect of the GPR30 agonist G1 on the expression of cardiac tissue-associated proteins and inflammation-related factors in OVX female mice with MI. (A) Representative blots. (B) TGF-β1 expression. (C) Collagen I expression. (D) BAX expression. (E) BCL-2 expression. (F) Caspase-3 expression. (G) p-AKT/AKT ratio. (H) TNF-α level. (I) IL-10 level. The results are expressed as the mean ± S.E.M. $^{a}p < 0.05$ and $^{aa}p < 0.01$ compared with the OVX group. $^{b}p < 0.05$ and $^{bb}p < 0.01$ compared with the OVX + MI group.

and C).

H&E staining revealed that the myocardial tissue in the infarct border zone in the MI group became slightly loose with a few cells arranged in disorder (Fig. 2A), whereas it was considerably loosened in the OVX group. In the OVX + MI group, the myocardial tissue in the infarction border zone was significantly loosened with increased disorder in cell arrangement.

We further detected changes in TGF-β1 expression, which is an indicator of the degree of myocardial fibrosis [33] (Fig. 2D and F). The apoptosis rate in the infarction border zone was examined by IF and TUNEL assay (Fig. 2D, E, and F). The MI and OVX treatments independently induced a higher apoptosis rate and fibrosis ($p < 0.05$ and $p < 0.01$ vs. control group, respectively). OVX combined with MI further increased the apoptosis rate and fibrosis in the myocardial tissue infarct border zone ($p < 0.05$ vs. MI group).

3.3. Effect of ovariectomy on myocardial fibrosis, apoptosis, and AKT-related protein expression

At 4 weeks after MI surgery, the expression of fibrosis-related proteins and apoptosis-related proteins in the myocardial tissue infarct border zone in OVX female mice was analyzed by WB (Fig. 3A). MI treatment did not induce an apparent change of GPR30 expression in the cardiac tissue of mice; however, in both the OVX group and OVX + MI group, GPR30 expression decreased significantly ($p < 0.05$ vs. control group; Fig. 3B). The expression of the fibrosis-related proteins TGF-β1 and collagen I in the myocardial tissue showed a consistent trend, with increased expression in the MI and OVX groups ($p < 0.01$ and $p < 0.05$ vs. control group, respectively); OVX combined with MI further increased TGF-β1 and collagen I expression ($p < 0.01$, vs. OVX group; Fig. 3C, D). Similarly, the apoptosis-related proteins BAX, BCL-2, and caspase 3 showed higher expression in the OVX + MI group than in the OVX group ($p < 0.05$ or $p < 0.01$; Fig. 3E, F, G). The pAKT/AKT ratio decreased in both the MI and OVX groups (vs. control group), and further decreased in the OVX + MI group ($p < 0.05$; Fig. 3H).

3.4. Effect of G1 on cardiac function of female mice with MI

On the basis of the results obtained from cardiac function and morphology analysis, we investigated the effect of the GPR30 agonist G1 on the cardiac function of OVX female mice with MI. Mice underwent MI surgery 2 weeks after they were OVX, and then, G1 was intraperitoneally injected for 4 weeks. M-mode ultrasonography revealed that both LVEF and LVFS values in the OVX + MI + G1 group increased significantly ($p < 0.01$ vs. OVX + MI group Fig. 4), along with higher dP/dt max values, suggesting that G1 improved cardiac function in OVXmice with MI.

3.5. Effect of G1 on myocardial fibrosis and morphological changes

Masson's trichrome staining showed that MI combined with OVX significantly decreased the thickness of the cardiac tissue and ventricular wall, and increased the degree of myocardial fibrosis ($p < 0.01$ vs. OVX group). However, addition of the agonist G1 decreased the degree of fibrosis in the myocardial tissue infarct border zone, and

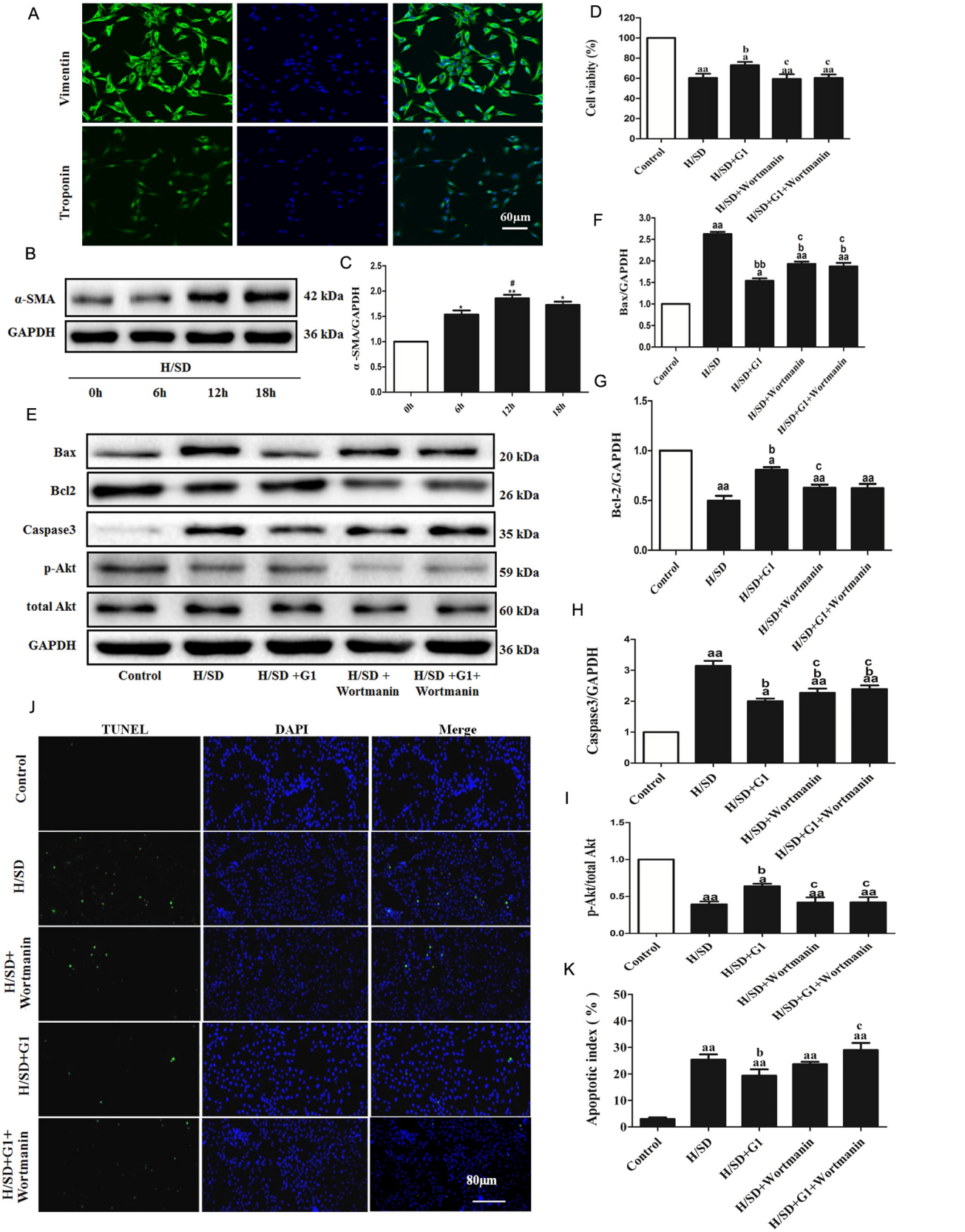

(caption on next page)

Fig. 7. Effects of the GPR30 agonist G1 on viability and apoptosis-related protein expression in hypoxia/serum-deprived cardiac fibroblasts (CFs). (A) Primary CFs express vimentin and are negative for troponin, consistent with the features of primary cultural cardiac fibroblasts (bar = 100 μm). (B) Representative blots. (C) α-SMA expression. (D) The viability of CFs was determined by MTT and was calculated by dividing the optical density of samples by the optical density of the sham control. (E) Representative blots. (F) BAX expression. (G) BCL-2 expression. (H) Caspase-3 expression. (I) p-AKT/AKT. (J) Representative photomicrographs of in situ detection of apoptotic cardiomyocytes by TUNEL staining. Green fluorescence shows TUNEL-positive nuclei; blue fluorescence shows nuclei of total cardiomyocytes. Original 400× magnification. (K) Percentage of TUNEL-positive nuclei. The results are expressed as mean ± S.E.M. $^{a}p < 0.05$ and $^{aa}p < 0.01$ compared with control group, $^{b}p < 0.05$ and $^{bb}p < 0.01$ compared with hypoxia/serum deprivation (H/SD) group, $^{c}p < 0.05$ and $^{cc}p < 0.01$ compared with H/SD + G1 group. (For interpretation of the references to color in this figure legend, the reader is referred to the web version of this article.)

reduced the ratio of fibrotic tissue ($p < 0.05$ vs. OVX + MI group, Fig. 5A, B, and C).

The morphological structure of the myocardial tissue infarct border zone was analyzed by H&E staining. Compared with the OVX group, OVX combined with MI caused the myocardial tissue to be loose and disordered, and edema was more obvious (Fig. 5A). Addition of G1 improved these parameters of myocardial tissue health in the infarct border zone in the OVX + MI group (Fig. 5A), indicating that G1 could improve the tissue structure in the myocardial tissue infarct border zone.

TUNEL staining and IFC assay showed that OVX combined with MI induced a high apoptosis rate and TGF-β1 expression in the myocardial tissue infarct border zone ($p < 0.01$ vs. OVX group). Additionally, the high apoptosis rate and TGF-β1 expression were reduced by G1 ($p < 0.01$ vs. OVX + MI group, Fig. 5D–F).

3.6. Effect of G1 on tissue fibrosis, apoptosis, expression of AKT-related proteins, and levels of inflammatory relative cytokines

WB revealed that G1 could affect the expression of fibrosis-related and apoptosis-related proteins in the myocardial tissue infarct border zone at 4 weeks after MI surgery in OVX female mice (Fig. 6A). Higher expression of TGF-β1 and collagen I in the myocardial tissue was detected in the OVX + MI group ($p < 0.01$ vs. OVX group). Additionally, the apoptosis-related proteins BAX and caspase-3 showed higher expression, but lower BCL-2 expression was detected in the myocardial tissue in the OVX + MI group ($p < 0.01$ vs. OVX group; Fig. 6D, E and F). The pAKT/AKT ratio in the OVX + MI group decreased ($p < 0.05$ vs. OVX group), and G1 intervention reversed this decrease (Fig. 6G). We also examined the levels of inflammatory cytokines in the serum of different groups. OVX combined with MI induced high levels of TNF-α and IL-10 ($p < 0.01$, vs. OVX group), and addition of G1 reduced the levels of these two inflammatory cytokines significantly ($p < 0.05$ vs. OVX + MI group) (Fig. 6H and I).

3.7. Effects of G1 on CFs under the H/SD condition simulating the in vivo ischemia model

Primary cultured CFs showed high vimentin expression and no troponin expression, consistent with their CF identity [34] (Fig. 7A). α-SMA expression in CFs after treatment with H/SD for different durations was evaluated. At 12 h, higher α-SMA expression in CFs treated with H/SD was detected ($p < 0.05$), whereas at 18 h no significant change was found (Fig. 7B and C). Thus, 12 h was chosen as the optimal duration for in vitro treatment with H/SD.

G1 treatment significantly increased the cell proliferation of H/SD-treated CFs ($p < 0.05$), and this increase was reversed by the PI3K inhibitor wortmanin (Fig. 6D). WB showed that G1 significantly decreased BAX and caspase-3 expression in the H/SD group ($p < 0.05$), but did not significantly change BAX and caspase-3 expression in the H/SD + wortmanin group (Fig. 7E, F, and H). Moreover, BCL-2 expression in the H/SD + G1 group was significantly higher than that in the H/SD group ($p < 0.05$; Fig. 7G). Although a high p-AKT/AKT ratio was detected in the H/SD + G1 group, addition of wortmanin caused the p-AT/AKT ratio to recover to a similar level as in the H/SD group (Fig. 7I). TUNEL assay demonstrated that G1 could significantly reduce the apoptosis rate of CFs treated with H/SD, and this reduction was inhibited by wortmanin (Fig. 7J and K).

4. Discussion

Estrogen exerts its biological effects mainly by binding to. ERs are divided into two categories: i) classic nuclear receptors, including ER-α and ER-β, which exhibit genotypic regulation by influencing the transcription of specific target genes; and ii) membrane receptors, including GPR30, which exhibit rapid non-genotype regulation mediated via the second messenger system [35]. GPR30 has cardiovascular protection effects, which can improve the cardiac function [16,36]. Lenhart et al. [37] reported that G1 treatment significantly reduced myocardial fibrosis in Ramp3+/+ and Ramp3−/− mice, which are susceptible to heart disease. Kang S et al. reported that chronic activation of GPR30 by its specific agonist G1 reduced post-ischemic dysfunction and infarct size after ischemia/reperfusion (I/R) [38]. However, the exact mechanism underlying this effect remains unclear.

Myocardial fibrosis is the main histological marker of cardiac dysfunction after MI [39]. Ventricular remodeling after MI includes apoptosis of myocardial cells, inflammation, hypertrophy, and synthesis and degradation of myocardial matrix collagen fibers [40]. Roy et al. [41] used chip technology to analyze gene expression in rat heart tissue 2 and 7 days after MI, and found that the differentially regulated genes were mainly associated with inflammation, apoptosis, and extracellular matrix. Kajstura et al. [42] found that myocardial cell apoptosis plays an important role in the development of MI. Apoptosis is a determinant of myocardial infarct size, and myocardial cell apoptosis in the infarct border zone is associated with infarct size [43,44]. Persistence of myocardial cell apoptosis increases the infarct size, causes progressive loss of myocardium, increases the infarct size, attenuates the ventricular wall, dilates the ventricles, and causes gradual cardiac remodeling, which develops into heart failure.

Removal of ovaries disrupts a number of hormonal pathways. However, mice after ovariectomy results in a lack of estrogen as well as postmenopausal women as previous report [45]. Our results showed that the values of LVEF and LVFS in the OVX group were significantly lower than that in the normal group. There are variations compared with previous studies [46–48] and this probably because we choose more old mice for ovariectomy. In this study, our main purpose is to clarify that estrogen reduction further aggravates MI-induced cardiac dysfunction. Mice were subjected to MI for 4 weeks. Echocardiography and pressure-volume catheter measurement showed a significant reduction in the cardiac function of the OVX female mice with MI, which consist with the results acquired previously [49,50]. Whereas IF results indicated significantly increased myocardial fibrosis ($p < 0.01$) and myocardial apoptosis ($p < 0.05$) in these mice, compared with that in non-OVX female mice with MI. These results suggest that estrogen deficiency aggravates cardiac injury in mice with MI. The considerable decrease in estrogen in postmenopausal women leads to reduced cardioprotection and increased risk for cardiovascular disease [14].

After MI, necrotic cells secrete inflammatory relative cytokines to trigger an inflammatory reaction, which causes myocardial fibrosis, ventricular remodeling, cardiac dysfunction, and eventually heart failure [51,52]. Those cytokines, such as TNF-α and IL-10 can regulate cell apoptosis through activation related signal pathways [53,54]. The

feedback of apoptosis can affect the severity of inflammation, and these two factors together affect the infarct size and cardiac function recovery [52]. Therefore, inhibiting inflammation and reducing apoptosis has become an important step in preventing ventricular remodeling and adjusting cardiac dysfunction after MI. Weil et al. [55] showed that GPR30 activation after myocardial I/R injury in rats significantly reduced the levels of TNF-α, IL-1, and IL-6 in the myocardium; relieved myocardial inflammation; and promoted the recovery of cardiac function. In our study, severe apoptosis and inflammation was observed after only 2 weeks in mice with MI, and the OVX mice with MI showed comparatively increased apoptosis and inflammation response. G1 treatment in OVX mice with MI reduced the apoptosis rate, induced low levels of TNF-α and high level of IL-10, decreased the degree of pericardial symphysis. Further study found that administration of G1 significantly enhanced cardiac function ($p < 0.05$), reduced the degree of myocardial fibrosis, and decreased myocardial infarct size ($p < 0.05$). These results preliminarily confirm that the GPR30 can improve cardiac function and reduce the degree of myocardial fibrosis in OVX female mice with MI.

The PI3K/AKT signaling pathway plays an important role in the regulation of inflammation and apoptosis [10,56]. Deschamps et al. [31] used the Langendorff model to observe the effect of G1 on rat cardiac I/R, and showed that G1 reduced the infarct size in rats. Furthermore, they found that GPR30 activation can cause phosphorylation of PI3K, AKT, and other intracellular kinases, suggesting that GPR30 activation exerts a cardioprotective effect through the PI3K/AKT signaling pathway. Therapeutic strategies targeting the PI3K/AKT pathway can achieve effective organ protection by activating a series of functional proteins that enhance proliferation and inhibit apoptosis, such as vascular endothelial growth factor and nuclear factor- κB [56,57]. The in vivo experiments in our study confirmed that G1 increases the p-AKT/AKT ratio in OVX mice with MI.

Furthermore, we used primary cultured CFs under H/SD to simulate the in vivo ischemia model. In particular, we investigated the effects of H/SD on apoptosis-related proteins in CFs. The results are consistent with those obtained from the in vivo experiment. However, when the PI3K/AKT pathway was blocked, G1 failed to cause significant changes in the expression of apoptosis-related proteins. Thus, it indicated that G1 inhibited the apoptosis of CFs by activating the PI3K/AKT signaling pathway, thereby mediated the myocardial protective effect of GPR30.

In conclusion, MI in OVX female mice causes ventricular wall thinning, ventricular dilatation, and cardiac remodeling, thus severely affecting cardiac function. GPR30 activation improves cardiac function via reducing apoptosis, myocardial tissue inflammatory response, infarct size, myocardial fibrosis, and ventricular remodeling. The in vitro results suggest that GPR30 may mediate myocardial protective effects through PI3K/AKT. Thus, GPR30 may be a new target for reducing myocardial infarct size and improving cardiac function in OVX female mice with MI.

Author contributions

Jincheng Liu, Shiqiang Yu, and Minggao Zhao conceived and designed the research; Xiaowu Wang, Linhe Lu, Yanzhen Tan and Liqing Jiang performed the experiments; Linhe Lu and Yanzhen Tan analyzed the data; Erhe Gao established the animal models; Xiaowu Wang, Linhe Lu and Jincheng Liu wrote the manuscript. All authors read the manuscript and approved the final version of the manuscript.

Conflicts of interest

The authors declare that there are no conflicts of interest.

Ethical approval

All animals used in this study were cared for in accordance with the Guide for the Care and Use of Laboratory Animals published by the United States National Institutes of Health (NIH publication number 85-23, revised in 2011), and all procedures were approved by the Committee of Experimental Animals of the FMMU.

Acknowledgements

This work was supported by the Natural Science Foundation of China (grant number 81570330 and 81770373).

References

[1] G. Rosano, C. Vitale, I. Spoletini, M. Fini, Cardiovascular health in the menopausal woman: impact of the timing of hormone replacement therapy, Climacteric 15 (2012) 299–305, https://doi.org/10.3109/13697137.2012.658899.
[2] V. Regitz-Zagrosek, Therapeutic implications of the gender-specific aspects of cardiovascular disease, Nat. Rev. Drug Discov. 5 (2006) 425–438, https://doi.org/10.1038/nrd2032.
[3] L. Fu, Y. Liu, J. Wang, Y. Sun, L. Zhang, T. Wu, et al., Cardioprotection by low-dose of estrogen and testosterone at the physiological ratio on ovariectomized rats during ischemia/reperfusion injury, J. Cardiovasc. Pharmacol. 70 (2017) 87–93, https://doi.org/10.1097/FJC.0000000000000497.
[4] A.Y. Chong, G.Y. Lip, Hormone replacement therapy and cardiovascular risk, Treat. Endocrinol. 1 (2002) 95–103.
[5] J.C. Bopassa, M. Eghbali, L. Toro, E. Stefani, A novel estrogen receptor GPER inhibits mitochondria permeability transition pore opening and protects the heart against ischemia-reperfusion injury, Am. J. Phys. Heart Circ. Phys. 298 (2010) H16–H23, https://doi.org/10.1152/ajpheart.00588.2009.
[6] M.R. Meyer, E.R. Prossnitz, M. Barton, The G protein-coupled estrogen receptor GPER/GPR30 as a regulator of cardiovascular function, Vascul. Pharmacol 55 (2011) 17–25, https://doi.org/10.1016/j.vph.2011.06.003.
[7] W.L. Li, W. Xiang, Y. Ping, Activation of novel estrogen receptor GPER results in inhibition of cardiocyte apoptosis and cardioprotection, Mol. Med. Rep. 12 (2015) 2425–2430, https://doi.org/10.3892/mmr.2015.3674.
[8] Z. Zhao, H. Wang, J.A. Jessup, S.H. Lindsey, M.C. Chappell, L. Groban, Role of estrogen in diastolic dysfunction, Am. J. Phys. Heart Circ. Phys. 306 (2014) H628–H640, https://doi.org/10.1152/ajpheart.00859.2013.
[9] D. Fan, Z. Yang, Y. Yuan, Q.Q. Wu, M. Xu, Y.G. Jin, et al., Sesamin prevents apoptosis and inflammation after experimental myocardial infarction by JNK and NF-kappaB pathways, Food Funct. 8 (2017) 2875–2885, https://doi.org/10.1039/c7fo00204a.
[10] G. Hu, X. Huang, K. Zhang, H. Jiang, X. Hu, Anti-inflammatory effect of B-type natriuretic peptide postconditioning during myocardial ischemia-reperfusion: involvement of PI3K/Akt signaling pathway, Inflammation 37 (2014) 1669–1674, https://doi.org/10.1007/s10753-014-9895-0.
[11] K. Nagaoka, T. Matoba, Y. Mao, Y. Nakano, G. Ikeda, S. Egusa, et al., A new therapeutic modality for acute myocardial infarction: nanoparticle-mediated delivery of pitavastatin induces cardioprotection from ischemia-reperfusion injury via activation of PI3K/Akt pathway and anti-inflammation in a rat model, PLoS One 10 (2015) e0132451, , https://doi.org/10.1371/journal.pone.0132451.
[12] X. Liu, C. Zhang, L. Qian, C. Zhang, K. Wu, C. Yang, et al., NF45 inhibits cardiomyocyte apoptosis following myocardial ischemia-reperfusion injury, Pathol. Res. Pract. 211 (2015) 955–962, https://doi.org/10.1016/j.prp.2015.09.018.
[13] Y. Wang, C. Li, K. Cheng, R. Zhang, K. Narsinh, S. Li, et al., Activation of liver X receptor improves viability of adipose-derived mesenchymal stem cells to attenuate myocardial ischemia injury through TLR4/NF-kappaB and Keap-1/Nrf-2 signaling pathways, Antioxid. Redox Signal. 21 (2014) 2543–2557, https://doi.org/10.1089/ars.2013.5683.
[14] E. Gao, Y.H. Lei, X. Shang, Z.M. Huang, L. Zuo, M. Boucher, et al., A novel and efficient model of coronary artery ligation and myocardial infarction in the mouse, Circ. Res. 107 (2010) 1445–1453, https://doi.org/10.1161/CIRCRESAHA.110.223925.
[15] Z. Liu, D. Yang, P. Xie, G. Ren, G. Sun, X. Zeng, et al., MiR-106b and MiR-15b modulate apoptosis and angiogenesis in myocardial infarction, Cellular Physiology and Biochemistry: International Journal of Experimental Cellular Physiology, Biochemistry, and Pharmacology 29 (2012) 851–862, https://doi.org/10.1159/000258197.
[16] X. Wang, Y. Tan, B. Xu, L. Lu, M. Zhao, J. Ma, et al., GPR30 attenuates myocardial fibrosis in diabetic ovariectomized female rats: role of iNOS signaling, DNA Cell Biol. 37 (2018) 821–830, https://doi.org/10.1089/dna.2018.4208.
[17] M. Itoga, Y. Konno, Y. Moritoki, Y. Saito, W. Ito, M. Tamaki, et al., G-protein-coupled estrogen receptor agonist suppresses airway inflammation in a mouse model of asthma through IL-10, PLoS One 10 (2015) e0123210, , https://doi.org/10.1371/journal.pone.0123210.
[18] E. Blasko, C.A. Haskell, S. Leung, G. Gualtieri, M. Halks-Miller, M. Mahmoudi, et al., Beneficial role of the GPR30 agonist G-1 in an animal model of multiple sclerosis, J. Neuroimmunol. 214 (2009) 67–77, https://doi.org/10.1016/j.jneuroim.2009.06.023.
[19] L. Tao, Y. Wang, E. Gao, H. Zhang, Y. Yuan, W.B. Lau, et al., Adiponectin: an indispensable molecule in rosiglitazone cardioprotection following myocardial infarction, Circ. Res. 106 (2010) 409–417, https://doi.org/10.1161/CIRCRESAHA.109.211797.

[20] B.N. Oskouei, G. Lamirault, C. Joseph, A.V. Treuer, S. Landa, J. Da Silva, et al., Increased potency of cardiac stem cells compared with bone marrow mesenchymal stem cells in cardiac repair, Stem Cells Transl. Med. 1 (2012) 116–124, https://doi.org/10.5966/sctm.2011-0015.

[21] K.E. Hatzistergos, E.C. Paulino, R.A. Dulce, L.M. Takeuchi, M.A. Bellio, S. Kulandavelu, et al., S-nitrosoglutathione reductase deficiency enhances the proliferative expansion of adult heart progenitors and myocytes post myocardial infarction, J. Am. Heart Assoc. 4 (2015), https://doi.org/10.1161/JAHA.115.001974.

[22] N.A. Trueblood, Z. Xie, C. Communal, F. Sam, S. Ngoy, L. Liaw, et al., Exaggerated left ventricular dilation and reduced collagen deposition after myocardial infarction in mice lacking osteopontin, Circ. Res. 88 (2001) 1080–1087, https://doi.org/10.1161/hh1001.090842.

[23] D. Wang, H. Zhu, Q. Yang, Y. Sun, Effects of relaxin on cardiac fibrosis, apoptosis, and tachyarrhythmia in rats with myocardial infarction, Biomedicine & Pharmacotherapy = Biomedecine & pharmacotherapie 84 (2016) 348–355, https://doi.org/10.1016/j.biopha.2016.09.054.

[24] L. Yu, Y. Sun, L. Cheng, Z. Jin, Y. Yang, M. Zhai, et al., Melatonin receptor-mediated protection against myocardial ischemia/reperfusion injury: role of SIRT1, J. Pineal Res. 57 (2014) 228–238, https://doi.org/10.1111/jpi.12161.

[25] L. Yu, H. Liang, Z. Lu, G. Zhao, M. Zhai, Y. Yang, et al., Membrane receptor-dependent Notch1/Hes1 activation by melatonin protects against myocardial ischemia-reperfusion injury: in vivo and in vitro studies, J. Pineal Res. 59 (2015) 420–433, https://doi.org/10.1111/jpi.12272.

[26] M. Al-Yahya, M. Raish, M.S. AlSaid, A. Ahmad, R.A. Mothana, M. Al-Sohaibani, et al., 'Ajwa' dates (Phoenix dactylifera L.) extract ameliorates isoproterenol-induced cardiomyopathy through downregulation of oxidative, inflammatory and apoptotic molecules in rodent model, Phytomedicine: International Journal of Phytotherapy and Phytopharmacology 23 (2016) 1240–1248, https://doi.org/10.1016/j.phymed.2015.10.019.

[27] R.K. Dubey, D.G. Gillespie, Z. Mi, E.K. Jackson, Exogenous and endogenous adenosine inhibits fetal calf serum-induced growth of rat cardiac fibroblasts: role of A2B receptors, Circulation 96 (1997) 2656–2666.

[28] D. Han, W. Huang, X. Li, L. Gao, T. Su, X. Li, et al., Melatonin facilitates adipose-derived mesenchymal stem cells to repair the murine infarcted heart via the SIRT1 signaling pathway, J. Pineal Res. 60 (2016) 178–192, https://doi.org/10.1111/jpi.12299.

[29] X. Li, D. Han, Z. Tian, B. Gao, M. Fan, C. Li, et al., Activation of cannabinoid receptor type II by AM1241 ameliorates myocardial fibrosis via Nrf2-mediated inhibition of TGF-beta1/Smad3 pathway in myocardial infarction mice, Cellular Physiology and Biochemistry: International Journal of Experimental Cellular Physiology, Biochemistry, and Pharmacology 39 (2016) 1521–1536, https://doi.org/10.1159/000447855.

[30] M.K. Dennis, R. Burai, C. Ramesh, W.K. Petrie, S.N. Alcon, T.K. Nayak, et al., In vivo effects of a GPR30 antagonist, Nat. Chem. Biol. 5 (2009) 421–427, https://doi.org/10.1038/nchembio.168.

[31] A.M. Deschamps, E. Murphy, Activation of a novel estrogen receptor, GPER, is cardioprotective in male and female rats, Am. J. Phys. Heart Circ. Phys. 297 (2009) H1806–H1813, https://doi.org/10.1152/ajpheart.00283.2009.

[32] Y. Yang, W. Duan, Z. Jin, W. Yi, J. Yan, S. Zhang, et al., JAK2/STAT3 activation by melatonin attenuates the mitochondrial oxidative damage induced by myocardial ischemia/reperfusion injury, J. Pineal Res. 55 (2013) 275–286, https://doi.org/10.1111/jpi.12070.

[33] Y. Guo, M. Gupte, P. Umbarkar, A.P. Singh, J.Y. Sui, T. Force, et al., Entanglement of GSK-3beta, beta-catenin and TGF-beta1 signaling network to regulate myocardial fibrosis, J. Mol. Cell. Cardiol. 110 (2017) 109–120, https://doi.org/10.1016/j.yjmcc.2017.07.011.

[34] Y. Bei, Q. Zhou, S. Fu, D. Lv, P. Chen, Y. Chen, et al., Cardiac telocytes and fibroblasts in primary culture: different morphologies and immunophenotypes, PLoS One 10 (2015) e0115991, , https://doi.org/10.1371/journal.pone.0115991.

[35] E.J. Filardo, P. Thomas, GPR30: a seven-transmembrane-spanning estrogen receptor that triggers EGF release, Trends Endocrinol Metab 16 (2005) 362–367, https://doi.org/10.1016/j.tem.2005.08.005.

[36] E.R. Prossnitz, M. Barton, The G-protein-coupled estrogen receptor GPER in health and disease, Nat. Rev. Endocrinol. 7 (2011) 715–726, https://doi.org/10.1038/nrendo.2011.122.

[37] P.M. Lenhart, S. Broselid, C.J. Barrick, L.M. Leeb-Lundberg, K.M. Caron, G-protein-coupled receptor 30 interacts with receptor activity-modifying protein 3 and confers sex-dependent cardioprotection, J. Mol. Endocrinol. 51 (2013) 191–202, https://doi.org/10.1530/JME-13-0021.

[38] S. Kang, Y. Liu, D. Sun, C. Zhou, A. Liu, C. Xu, et al., Chronic activation of the G protein-coupled receptor 30 with agonist G-1 attenuates heart failure, PLoS One 7 (2012) e48185, , https://doi.org/10.1371/journal.pone.0048185.

[39] Y. Huang, Y. Qi, J.Q. Du, D.F. Zhang, MicroRNA-34a regulates cardiac fibrosis after myocardial infarction by targeting Smad4, Expert Opin. Ther. Targets 18 (2014) 1355–1365, https://doi.org/10.1517/14728222.2014.961424.

[40] F. Kuwahara, H. Kai, K. Tokuda, M. Takeya, A. Takeshita, K. Egashira, et al., Hypertensive myocardial fibrosis and diastolic dysfunction: another model of inflammation? Hypertension 43 (2004) 739–745, https://doi.org/10.1161/01.HYP.0000118584.33350.7d.

[41] S. Roy, S. Khanna, D.E. Kuhn, C. Rink, W.T. Williams, J.L. Zweier, et al., Transcriptome analysis of the ischemia-reperfused remodeling myocardium: temporal changes in inflammation and extracellular matrix, Physiol. Genomics 25 (2006) 364–374, https://doi.org/10.1152/physiolgenomics.00013.2006.

[42] J. Kajstura, W. Cheng, K. Reiss, W.A. Clark, E.H. Sonnenblick, S. Krajewski, et al., Apoptotic and necrotic myocyte cell deaths are independent contributing variables of infarct size in rats, Laboratory Investigation; A Journal of Technical Methods and Pathology 74 (1996) 86–107.

[43] M. Arakawa, M. Yasutake, M. Miyamoto, T. Takano, S. Asoh, S. Ohta, Transduction of anti-cell death protein FNK protects isolated rat hearts from myocardial infarction induced by ischemia/reperfusion, Life Sci. 80 (2007) 2076–2084, https://doi.org/10.1016/j.lfs.2007.03.012.

[44] A. Lazou, E.K. Iliodromitis, D. Cieslak, K. Voskarides, S. Mousikos, E. Bofilis, et al., Ischemic but not mechanical preconditioning attenuates ischemia/reperfusion induced myocardial apoptosis in anaesthetized rabbits: the role of Bcl-2 family proteins and ERK1/2, Apoptosis: An International Journal on Programmed Cell Death 11 (2006) 2195–2204, https://doi.org/10.1007/s10495-006-0292-5.

[45] Y. Kamei, M. Suzuki, H. Miyazaki, N. Tsuboyama-Kasaoka, J. Wu, Y. Ishimi, et al., Ovariectomy in mice decreases lipid metabolism-related gene expression in adipose tissue and skeletal muscle with increased body fat, J. Nutr. Sci. Vitaminol. 51 (2005) 110–117.

[46] S. Ahmad, X. Sun, M. Lin, J. Varagic, G. Zapata-Sudo, C.M. Ferrario, et al., Blunting of estrogen modulation of cardiac cellular chymase/RAS activity and function in SHR, J. Cell. Physiol. 233 (2018) 3330–3342, https://doi.org/10.1002/jcp.26179.

[47] J.S. da Silva, D. Gabriel-Costa, H. Wang, S. Ahmad, X. Sun, J. Varagic, et al., Blunting of cardioprotective actions of estrogen in female rodent heart linked to altered expression of cardiac tissue chymase and ACE2, J. Renin-Angiotensin-Aldosterone Syst. 18 (2017) 147032031772227, , https://doi.org/10.1177/1470320317722270.

[48] A.K.N. Alencar, G.C. Montes, D.G. Costa, L.V.P. Mendes, A.M.S. Silva, S.T. Martinez, et al., Cardioprotection induced by activation of GPER in ovariectomized rats with pulmonary hypertension, J. Gerontol. A Biol. Sci. Med. Sci. 73 (2018) 1158–1166, https://doi.org/10.1093/gerona/gly068.

[49] T. Knezevic, V.D. Myers, F. Su, J. Wang, J. Song, X.Q. Zhang, et al., Adeno-associated virus serotype 9 - driven expression of BAG3 improves left ventricular function in murine hearts with left ventricular dysfunction secondary to a myocardial infarction, JACC Basic to Translational Science 1 (2016) 647–656, https://doi.org/10.1016/j.jacbts.2016.08.008.

[50] S. Sivasinprasasn, P. Tanajak, W. Pongkan, W. Pratchayasakul, S.C. Chattipakorn, N. Chattipakorn, DPP-4 inhibitor and estrogen share similar efficacy against cardiac ischemic-reperfusion injury in obese-insulin resistant and estrogen-deprived female rats, Sci. Rep. 7 (2017) 44306, , https://doi.org/10.1038/srep44306.

[51] P.W.M. Fedak, S. Verma, R.D. Weisel, R.-K. Li, Cardiac remodeling and failure from molecules to man (part II), Cardiovascular Pathology: The Official Journal of the Society for Cardiovascular Pathology 14 (2005) 49–60.

[52] P. Sirish, N. Li, J.Y. Liu, K.S. Lee, S.H. Hwang, H. Qiu, et al., Unique mechanistic insights into the beneficial effects of soluble epoxide hydrolase inhibitors in the prevention of cardiac fibrosis, Proc. Natl. Acad. Sci. U. S. A. 110 (2013) 5618–5623, https://doi.org/10.1073/pnas.1221972110.

[53] R. Zhang, Y. Xu, N. Ekman, Z. Wu, J. Wu, K. Alitalo, et al., Etk/Bmx transactivates vascular endothelial growth factor 2 and recruits phosphatidylinositol 3-kinase to mediate the tumor necrosis factor-induced angiogenic pathway, J. Biol. Chem. 278 (2003) 51267–51276, https://doi.org/10.1074/jbc.M310678200.

[54] P. Krishnamurthy, J. Rajasingh, E. Lambers, G. Qin, D.W. Losordo, R. Kishore, IL-10 inhibits inflammation and attenuates left ventricular remodeling after myocardial infarction via activation of STAT3 and suppression of HuR, Circ. Res. 104 (2009) e9–18, https://doi.org/10.1161/CIRCRESAHA.108.188243.

[55] B.R. Weil, M.C. Manukyan, J.L. Herrmann, Y. Wang, A.M. Abarbanell, J.A. Poynter, et al., Signaling via GPR30 protects the myocardium from ischemia/reperfusion injury, Surgery 148 (2010) 436–443, https://doi.org/10.1016/j.surg.2010.03.011.

[56] D.L. Williams, T. Ozment-Skelton, C. Li, Modulation of the phosphoinositide 3-kinase signaling pathway alters host response to sepsis, inflammation, and ischemia/reperfusion injury, Shock 25 (2006) 432–439, https://doi.org/10.1097/01.shk.0000209542.76305.55.

[57] R. Aneja, P.W. Hake, T.J. Burroughs, A.G. Denenberg, H.R. Wong, B. Zingarelli, Epigallocatechin, a green tea polyphenol, attenuates myocardial ischemia reperfusion injury in rats, Molecular Medicine (Cambridge, Mass) 10 (2004) 55–62.